PHYSICAL MODELS FOR SOIL SALINITY MAPPING OVER ARID LANDSCAPE USING LANDSAT-OLI AND FIELD DATA: VALIDATION AND COMPARISON

Z. Al-Ali [1], A. Bannari [1-2], N. Hameid [2] and A. El-Battay [3]

[1] Department of Natural Resources and Environment,
[2] Department of Geoinformatics,
College of Graduate Studies, Arabian Gulf University, Manama, P.O. Box: 26671, Kingdom of Bahrain,
Tel: (973) 1723-9545; Fax: (973) 1723-9552; E-mail: abannari@agu.edu.bh
[3] International Center for Biosaline Agriculture (ICBA), Dubai, United Arab Emirates

Abstract

The aim of the present study is focusing on a validation and comparison among eight different physical models for soil salinity mapping in arid landscape. The considered models were developed for different geographic regions around the world, i.e. Latino-America (Mexico), Middle-East (Iraq), north and east Africa (Morocco and Ethiopia) and Asia (China). These models integrated different spectral bands and unlike mathematical functions in their conceptualization (stepwise, linear, second order, logarithmic, and exponential). Three main steps were considered. The Landsat-OLI image data was radiometrically standardized and the models were implemented to derive soil salinity maps. The field survey was organized during 4 days, two days before the OLI data acquisition, and a total of 100 soil samples were collected representing different salinity levels, and each sampling location was geographically localized using accurate GPS. The laboratory analysis was accomplished to derive electrical conductivity (EC-Lab) for validation purposes. Statistical analysis ($p < 0.05$) was applied between predicted salinity maps (EC-Predicted) and the measured ground truth (EC-Lab). The results obtained showed that predictive models based on VNIR bands and vegetation indices are inadequate for soil salinity prediction due to a serious signals confusion between the salt-crust and the soil optical properties in these spectral bands. The statistical tests revealed insignificant fits ($R^2 \leq 0.41$) with a very high prediction errors (RMSE ≥ 0.65). While, the model based on second order polynomial function and integrating the SWIR bands provides results of best fitness in comparison to the ground truth, yielding an R^2 of 0.97 and low overall RMSE of 13%.

Index Terms: Soil Salinity, Physical models, Validation, Electrical conductivity, Remote sensing, Landsat-OLI.

1. INTRODUCTION

Drylands are seriously facing challenge of spatial and temporal distribution of soil salinity during drought periods [1], due to water quality and scarcity beside the increase in an evapotranspiration rates [2]. Salinized soils covered 40 to 45% of the Earth land and extensively occur in Africa and Asia [3, 4]. In addition to water stress, these lands are vulnerable to marginality and desertification as a result of human activities [5] and global climate change impact [5, 6]. Obviously, these factors have significant impacts on land degradation, crop production, economic aspects and infrastructure [7]; as well as ecosystem functionality, human wellbeing and sustainable development.

Soil salinity is a dynamic phenomenon and it must be monitored in space and time [8, 9]. Globally, measuring electrical conductivity extracted from a saturated soil paste at the laboratory (EC-Lab) is the most accurate method used for soil salinity mapping. Unfortunately, this method is expensive and time consuming, especially for regular monitoring over a long period, and for comparisons over large areas [8, 10]. Thus, remote sensing and GIS offer advantages over ground-based methods [9, 11-13] these methods make it possible to map vast areas that are subject to soil salinity hazards on spatial and temporal

bases with good accuracy. Several physical models were developed for salt-affected soil mapping in different geographic regions around the world (i.e. Latino-America, Middle-East, north and east Africa, and Asia using remote sensing [9, 12-14].

The aim of the present study is concerning with a validation and comparison among eight different physical models for soil salinity mapping in arid landscape. The methodology is based on three main steps including field survey for soil sampling, laboratory analysis to derive EC-Lab for validation purposes, and Landsat-OLI image preprocessing and processing. Statistical analysis was applied between predictive salinity values derived from OLI image and the observed values (ground truth) derived from the laboratory analysis.

2. MATERIALS AND METHODS

2.1. Study site

The state of Kuwait situated in the north western part of the Arabian Peninsula (28° 45' to 30° 06' N, 46° 33' to 48° 35' E) is characterized by arid climate, very hot summers (46.8°C) and the rainfall is irregular in amount, frequency and distribution with a mean annual of 118 mm. The main geomorphological Features are Wadis, escarpments, sand dunes, Sabkhas, depressions, playas and alluvial fans [15, 16]. These Features are controlled by three types of surface deposits [17]. First, Aeolian deposits such as dunes and sand sheet. Second, evaporates such as gypsum ($CaSO_4.2H_2O$) and anhydrite ($CaSO_4$), and other salts deposits in coastal and inland Sabkhas. Third, fluvial deposits such as pebbles and gravels along the Wadi Al-Batin channel. Each of these deposits has specific geomorphic characteristics based on their origin, topography that is generally flat with low relief, and climatic impacts [15]. Geologically, Kuwait stratigraphy consists of two Stratigraphic Groups; Kuwait Group and Hasa Group [18] consisting of six Formations, four of them are exposed in the outcrops represented by Dammam, Ghar, Mutla and Jal-AzZor Formation. Dammam Formation from Hasa Group *(Eocene)* consists of white fine grained cherty limestone and form some karst. The three other Formations are composed mostly of sandy limestone, calcareous sandstones, sand and clay. Soils of Kuwait are mostly sandy with limited organic matter, very low nutrient and very high amount of calcareous materials. Moreover, Gatch layer occur in many Kuwaiti soil, which is considered a calcic and/or gypsic pan [19].

2.2. Field work and laboratory analysis

According to the United States Department of agriculture [20], soil of Kuwait have been classified into two main groups; the Aridisols constituting 70.8% and the Entisols forming 29.2%, while the other restricted and marginal groups are representing the remaining percentage (6.64%). These two major groups are consisted of eight major classes based on morphology, mineralogical, chemical and physical characteristics [20].The extreme salinity class (Sabkhas) occur in Aquisalid soil on coastal flats and inland Playas, which contains significant content of salts and gypsum. High salinity class arise in Haplocalcide soil that attribute to layer of carbonate masses and medium gypsum content. Moderate to low salinity class occur in Petrocalcide soil, which characterised of well to moderately drained,

shallow rooting depth, calcic hardpan overlying sandy to loamy soils and presence of scattering halophytic plants. Based on the field work and soil map, the following soil salinity classes were considered: non-saline, low, moderate, high, very high, and extreme salinity. A total of 100 soil samples representing these six salinity classes were collected during four days, 15th -18th May 2017 (dry season). Samples were collected from upper layer of the soil (5 to 10 cm deep), placed and numbered in plastic bags. In addition, each soil sample was physically described (color, brightness, texture, etc.), photographed, and geographically localized using accurate Global Position System (GPS, $\sigma \leq \pm 30$ cm) for validation step.

In the laboratory, the considered soil samples were dried, grind, and sieved using 2 mm sieve. The saturated soil past extract method was utilized to measure the EC$_{-Lab}$ and pH. Moreover, the major soluble cations (Ca^{2+}, Mg^{2+}, Na^+, and K^+) and anions (Cl^- and SO_4^{2-}) were identified, and the sodium adsorption ratio (SAR) and exchangeable sodium percentage (ESP) were calculated. These analyses have been carried out at the soil laboratory using methods that meet the current international standards in soil science [21].

2.3. Image data preprocessing

The used Landsat-OLI image was acquired the 13th of May 2017, two days before the field work campaign for soil sampling. Before any processing operation and accurate information extraction, preprocessing steps are required [22, 23]. These steps are related to sensor-drift radiometric calibration and atmospheric corrections (scattering and absorption) [23, 24]. The *Canadian Modified Simulation of the Satellite Signal in the Solar Spectrum* (CAM5S), based on the *Herman radiative transfer code* [25], was applied for atmospheric parameter simulation. For sensor calibration, the solar zenith angle values and absolute calibration parameters (gain and offset) delivered by USGS-EROS Center were applied. Sensor calibration and atmospheric interferences were combined and corrected in one-step using PCI-Geomatica [26] to preserve the radiometric integrity of our image data.

2.4. Physical models and image processing

Soil salinity is modeled for regional and global scales around the world considering several environment, and using moderate or coarse spatial resolution, i.e., Landsat or MODIS [12, 27]. Consequently, numerous empirical, semi-empirical and physical models were developed. The present study is the first attempt to validate and compare eight models developed for salt-affected soil mapping in semi-arid and arid regions, i.e. Latino-America, Middle-East, Africa and Asia [12, 27, 28]. In addition to the geographic location, the selection is also based on the difference of the mathematical models that are integrated in their conceptualization: stepwise, linear, second order polynomial, logarithmic, and exponential functions.

For a Mexican environment, the first developed model is based on exponential function [28] integrating in its equation the spectral responses of the bar soil and the vegetation cover fraction calculated using *Normalized Difference Vegetation Index* (NDVI) and *Combined Spectral Response Index* (CORSI). The second model was developed to map spatiotemporal soil salinity variation of irrigated agricultural land in Morocco based on the first linear regression and integrating the four visible spectral bands of Landsat-OLI [29]. For Ethiopian agricultural land, the third proposed model is also based on linear regression integrate the near-infrared (NIR) and red spectral bands [30]. The fourth model was developed to map the largest sada saline-alkali regions worldwide in China [11] by exploring only the blue band and the stepwise linear regression.

The fifth, sixth, and seventh models were developed for arid land in Iraq [27] considering only the red and NIR bands but with certain particular difference conditions in term of experimentation for a specific scales and applications. Indeed, the fifth model was developed for regional scale based on a logarithmic function, integrating the soil apparent salinity (EM$_V$) measured in vertical direction and the vegetation cover information based on *Generalized Difference Vegetation Index* (GDVI). The sixth model is a simple linear logarithmic model based only on GDVI and do not consider EM$_V$ variable. Whereas, developed specifically for local scale and considering vegetated areas, the seventh model relies on both

logarithmic and exponential functions integrating the GDVI and the apparent soil salinity (EM$_H$) measured in the horizontal direction. Finally, in semi-arid environment in Morocco, the eighth model was developed for slight and moderate salinity prediction of agricultural land based on the SWIR spectral bands, EC$_{-Lab}$ and a second order polynomial function [12]. Tested in Middle-East, this model discriminate significantly among several soil salinity classes and highlight remarkably the Sabkhas areas, i.e. extreme salinity [14, 31]. All these considered models were implemented and calculated using EASI-modeling of PCI-Geomatica image processing software [26].

$$\text{Model}_{-1} = 348.104 * \text{Exp}^{-18.372 * \text{COSRI}} \quad (1)$$
$$\text{COSRI} = \left(\frac{B + G}{R + NIR}\right) * NDVI$$
$$NDVI = (NIR - R)/(NIR + R)$$

$$\text{Model}_{-2} = 13.56 * OLI_{-SI} - 2.24 \quad (2)$$
$$OLI_{-SI} = (CB^2 * 50) - (B + G + R)$$

$$\text{Model}_{-3} = -0.706 + 7.519 * SI \quad (3)$$
$$SI = \sqrt{R * NIR}$$

$$\text{Model}_{-4} = -3.35 + 0.56 * B \quad (4)$$

$$\text{Model}_{-5} = 0.0005 * EM_V^2 - 0.0779 * EM_V + 12.655 \quad (5)$$
$$EM_V = 66.338 - 258.114 * \ln(GDVI)$$
$$GDVI = (NIR^2 - R^2)/(NIR^2 + R^2)$$

$$\text{Model}_{-6} = -2.87 - 23.27 * \ln(GDVI) \quad (6)$$

$$\text{Model}_{-7} = 0.0002 * EM_H^2 + 0.0956 * EM_H + 0.0688 \quad (7)$$
$$EM_H = -606.197 - 460.03 * \ln(GDVI) + 245.086 * \text{Exp}(GDVI)$$

$$\text{Model}_{-8} = C^{ste} * [4521 * (SSSI2)^2 + 124.50 * (SSSI2) + .41] \quad (8)$$
$$SSSI2 = \frac{(SWIR1 * SWIR2) - (SWIR2 * SWIR2)}{SWIR1}$$

Where C, B, G, R and NIR are the ground reflectance in the costal, blue, green, red and near-infrared spectral bands, respectively. The SWIR1 and SWIR2 are the ground reflectance in shortwave infrared spectral bands, i.e., OLI-6 and OLI-7 bands, respectively. *SI* means a salinity index. C^{ste} is a scaling factor between the ground based-measurements and the use of satellite image data (must be calculate for each application case) [31].

2.5. Statistical analysis

The coefficient of determination (R^2) and root mean square error (RMSE) were determined to assess the performance of the considered salinity models. Whereas, R^2 explains the variance of fit between EC$_{-Lab}$ and EC$_{-Predicted}$ values. The RMSE is an indicator for model errors and performance [32], it's a residual error estimating the absolute error between EC$_{-Lab}$ and EC$_{-Predicted}$ values. These two variables were calculated using the following equations:

$$R^2 = 1 - \frac{\sum_{i=1}^{n}(y - y')^2}{\sum_{i=1}^{n}(y' - \bar{Y})^2} \quad (9)$$

$$RMSE = \sqrt{\frac{\sum_{i=1}^{n}(y - y')^2}{n}} \quad (10)$$

Where Y is the EC$_{-Lab}$ values, y' is the EC$_{-Predicted}$, $\bar{Y}$ is the average of observed values, and n is the number of observations.

3. RESULTS ANALYSIS AND DISCUSSION

The major cations (Ca^{2+}, Mg^{2+}, Na^+ and K^+) and anions (Cl^- and SO_4^{2-}), pH, EC$_{-Lab}$ and SAR values were determined in the laboratory from saturated soil paste extract. Table 1 summarizes the six classes of salinity according to the EC$_{-Lab}$ values and present the mean values of cation and anion elements in each class. Over the considered study site, these classes areas occupied 51.4%, 30%, 12.9%, 2.9%, 1.4%

and 1.4% for non-saline, extreme, low, moderate, high and very high salinity, respectively. According to the laboratory analysis, the soil samples are in general highly affected by chloride (Cl^-) and sodium (Na^+), magnesium (Mg^{2+}) and calcium (Ca^{2+}) than other elements. Besides, the EC-Lab and SAR are increased gradually and very largely from non-saline (EC-Lab: 2.6 dS.m^{-1}, SAR: 3.4) to extreme salinity in Sabkha (EC-Lab: 400 dS.m^{-1}, SAR: 166.5). Obviously, these results are in agreement with the predicted salinity classes ascertained by remote sensing image processing. Sequentially, the soil pH values in the range from 7 to 7.7 indicated slightly alkaline reaction due to the preponderance of bicarbonate (HCO^-_3) in the soils with a range from 4 to 10 meq^{-1}.

Table 1: Laboratory analysis of different soil classes.

Salinity classes	EC-Lab dSm^{-1}	pH	Ca^{2+}	K$^+$	Mg^{2+}	Na$^+$	Cl$^-$	HCO$_3$	SAR
Non-Saline	2.6	7.6	39	1.8	7.8	32	9.6	6.6	3.4
Low	6.7	7.7	67	2.3	12	23	38	9.1	3.5
Moderate	11.8	7.7	45	7	14	49	70	10	9.1
high	38.4	7.3	146	310	100	258	350	6	23.3
Very high	48.8	7.4	78	15	19	325	590	4	46.8
Extreme	400.3	7.0	230.5	97	1118	3615	3932	6.6	166.5
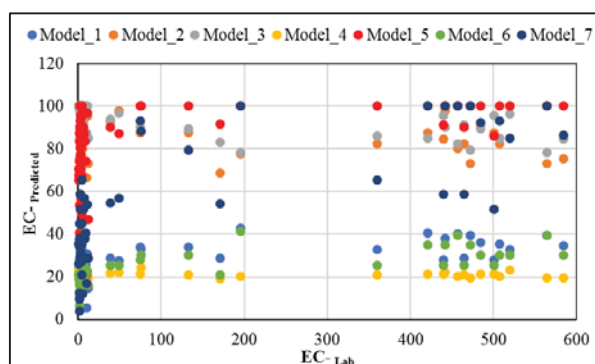
Fig.1. Relationship between EC_Lab and EC_Predicted derived from models 1 to 7.
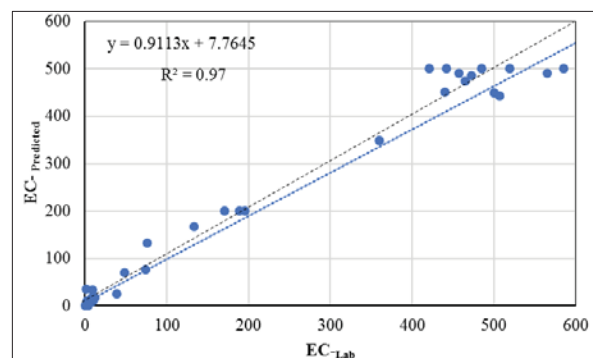
Fig.2. Relationship between EC-Lab and EC-Predicted derived from model-8.

Figs. 1 and 2 illustrate the relationship between EC-Lab and EC-Predicted derived from the considered 8 models [full set of results for all models are not shown separately due to space limit]. This validation procedure highlight the potential and the limit of each model separately. The first major observation is that except the model-8, all the other models displayed in Fig. 1 are not following the regular and logic linear fit 1:1 line, i.e., f(x) = x. A serious strong overestimation are observed for non-saline or low salinity and very significant saturation was found for high to extreme salinity classes. For instance, the model-4 based on the blue band only showed very low regression fitness (R^2 of 0.18) and a very high RMSE (77%). Independently to

the soil salinity class ($1.3 \leq$ EC-Lab $\leq$ 600 dS.m^{-1}), its predicted values oscillate only around 20 dS.m^{-1}, which represents a very wrong prediction. This result was anticipated because well know that the blue band is very sensitive to the variation of soil characteristics (color, brightness, texture, etc.) which limit the discrimination of soil-salinity classes [10, 13]. For tiny bits such finding could be attributed to dust and water vapor in the air, and even by air molecules themselves than the longer wavelengths. In addition, during the conceptualization of most remote sensing sensors such as Landsat-OLI, this spectral domain is dedicated especially for two specific applications: shallow water and tracking fine particles like dust and smoke in the atmosphere and not for soil mineralogy detection and mapping. Likewise, the model-2 based on the four visible bands of OLI predict the ground truth with low regression fitness (R^2 of 0.21) and very high RSME (72%). Moreover, its prediction values were varied between 65 and 100 dS.m^{-1} for non-saline soil (EC-Lab $\leq$ 8 dS.m^{-1}) and Sabkha with pure salt (400 to 600 dS.m^{-1}), respectively. These overestimation and underestimation results are in agreement with other relevant studies that have demonstrated the limit of the visible bands for discrimination of soil salinity classes [13].

Model-1 and model-5 are, respectively, based on exponential and logarithmic functions. They integrate both the bar soil spectral responses and the vegetation cover fraction derived from NDVI and GDVI based on VNIR bands. Such spectral domains make the two models very sensitive to the soil color and brightness [31]. Hence, this situation introduces very severe confusion and ambiguity between the predicted soil salinity classes. Both models provide similar results showing insignificant coefficient of determination ($R^2 \leq$ 0.23) and very high RMSE (70%). Moreover, the non-saline (EC-Lab $\leq$ 8 dS.m^{-1}) and extreme salinity (EC-Lab $\geq$ 400 dS.m^{-1}) classes are, respectively, overestimated and underestimated. Model-1 predicts the range of EC for extreme classes between 5 and 40 dS.m^{-1}, while the prediction of model-5 was located between 40 and 100 dS.m^{-1}. Similar behaviour and finding has been obtained for model-3. Compared to ground truth (EC-Lab), the prediction produced by model-3 is not corresponding to the soil salinity classes where the regression fitness value was relatively low (R^2 of 0.41) concurrent with a very high RMSE (72%). Confision occurred for soil classes of low salinity or non-saline (EC-Lab $\leq$ 12 dS.m^{-1}) that were predicted with very high range (65 to 100 dS.m^{-1}). A very severe saturation was also observed for soil classes of high salinity that have been predicted with a range between 80 and 100 dS.m^{-1}, while the estimation based on ground truth (EC-Lab) found to be ranged between 100 and 600 dS.m^{-1}.

The model-6 based on a linear logarithmic function integrating the GDVI for salt-affected soil detection at the regional scale also described the salinity classes with very significant uncertainty levels. The statistical analysis revealed that R^2 was equal to 0.38 concurrent with very strong RMSE (75%). Noticeably, this model showed an overestimate particularly for non-saline soil class with a range values between 6 to 45 dS.m^{-1}. Contrariwise, exhibited underestimate for the high, very high and extreme salinity classes with a low range between 25 and 40 dS.m^{-1}. Proposed specifically for local scale, the model-7 based on a combination of logarithmic and exponential functions integrating GDVI and the EM$_H$ was fit with relatively an acceptable coefficient of determination (R^2 of 0.54), but unfortunately the calculated RMSE remains very high (65%). This model showed a similar trend so that of model-6, classifying the validation points in two dominant groups. The first group represents mixed randomly together the first five salinity classes (non-saline, low, moderate, high, and very high) with distinguished overestimation by predicting the range of EC between 0 and 60 dS.m^{-1}. While, the second group was isolated by a single soil class representing the extreme salinity class that was predicted by a low range varied from 60 to 100 dS.m^{-1}. Obviously, these results are contradict to those observed at the field.

The first seven models (1 to 7) have failed to predict correctly and accurately soil salinity classes in arid landscape. The reason behind this failure reside in the integration of VNIR bands and vegetation indices (NDVI, COSRI and GDVI) in the modeling concepts of these models. Obviously, several studies based on field, laboratory, and real satellite data acquired with several sensors (TM, ETM+, OLI, ALI EO-1, Sentinel-MSI, andWorldView-3) revealed that the VNIR spectral domain lack the required sensitivity for accurate soil salinity discrimination and quantification. In such wavelengths, the main factors affecting the soil spectral signatures are the salt types, soil

mineralogy, level of moisture, organic matter content, color and brightness, roughness, and vegetation cover. Undoubtedly, these factors influence the signal gathered by the sensor in a specific pixel size causing severe confusion between the salt-crust in the soils and the intrinsic soil optical properties [8,10,13,33].

Finally, the model-8 integrating the SWIR bands, which are sensitive to soil-salt mineralogy, provides the best result of regression fitness with R^2 of 0.97 and low RMSE of 0.13 at significance level of $p < 0.05$. The scatter-plot illustrated in Fig. 2 reveals a good linear relationship between the EC_{-Lab} and $EC_{-Predicted}$ in term of good fit 1:1 showing an excellent spatial variability of salinity ($1.3 \leq EC_{-Lab} \leq 400$ dSm^{-1}). In spite of this model was developed for slight and moderate salinity [12], the present study showed an appropriate prediction for the different salinity classes investigated. However, slight overestimation is observed for high to very high salinity classes with the EC_{-Lab} range from 50 to 170 $dS.m^{-1}$, as well as less underestimation (or saturation) was pointed out for the extreme salinity classes ($\geq$ 400 $dS.m^{-1}$). Indeed, this underestimation is attributed to the impact of soil moisture in Sabkha and shorelines (that are very salty) on the signal recorded by the SWIR bands that are considerably sensitive to moisture. While, the slight overestimation it could be due the scale factor that was estimated between field samples identified from an area about 50 x 50 cm^2 and its homologous points in the OLI image represented by 900 m^2 pixel size. In addition, the preprocessing steps of OLI data are essential for the removal of sensor artifacts and atmospheric interference effects. Moreover, it is probable that residual errors persist (because each spectral band was corrected uniformly and not pixel-by-pixel), causing a small difference between the EC_{-Lab} measured at the laboratory and the homologous $EC_{-Predicted}$ calculated from remote sensing image. Eventually, despite these variations, the validation of model-8 provides satisfactory results in comparison to the other 7 models.

4. ACKNOWLEDGEMENTS

5. REFERENCES

[1] Dai, A. "Drought under Global Warming: A Review". WIREs Climate Change, 2, 45–65, 2011.

[2] Kurylyk, B. and MacQuarrie, K. "The Uncertainty Associated with Estimating Future Groundwater Recharge: A Summary of Recent Research and an Example from a Small Unconfined Aquifer in a Northern Humid-Continental Climate". *J. of Hydrology, 492,* 244-253, 2013.

[3] GDA. "Doha to Host the Global Dryland Alliance Founding Conference". Retrieved from Global Dryland Alliance, 2017: http://www.globaldrylandalliance.org/en/doha-to-host-the-global-dryland-alliance-founding-conference/

[4] White, R. *et al.* "An Ecosystem Approach to Drylands: Building Support for New Development Policies, Information Policy Brief No.1". Washington DC, USA: World Research Institute, 2002.

[5] Shahid, S. and Al-Shankiti, A. "Sustainable Food Production in Marginal Lands-Case of GDLA Member Countries". *Int. Soil and Water Conservation Research*, 1(1), 24-38, 2013.

[6] Teh, S. and Koh, H. "Climate Change and Soil Salinization: Impact on Agriculture, Water and Food Security". *Int. J. of Agriculture, Forestry and Plantation, 2,* 1-9, 2016.

[7] Naing O, A. *et al.* "Food Security and Socio-economic Impacts of Soil Salinization in Northeast Thailand". *Int. J. of Environmental and Rural Development,* 4(2), 2013.

[8] Metternicht, G. and Zinck, J. "Remote Sensing of Soil Salinization: Impact on Land Management". Boca, Raton, 374: CRC Press Taylor and Francis Group, 450 pages, 2009.

[9] Allbed, A. and Kumar, L. "Soil Salinity Mapping and Monitoring in Arid and Semi-Arid Regions Using Remote Sensing Technology: A Review". *Adv. in Remote Sensing,* 2, 373-385, 2013.

[10] Metternicht, G. and Zinck, J. "Remote Sensing of Soil Salinity: Potentials and Constraints". *R. S. of Envir.,* 85, 1-20, 2003.

[11] Bai, L. *et al.* "Remote Sensing of Soil Alkalinity and Salinity in the Wuyuer-Shuangyang River Basin, Northeast China". *Remote Sensing, 8 (163),* 1-16, 2016.

[12] Bannari, A. *et al.* "Mapping Slight and Moderate Saline Soils in Irrigated Agricultural Land Using Advanced Land Imager Sensor (EO-1) Data and Semi-Empirical Models". *Com. in Soil Science and Plant Analysis Journal,* 47, 1883-1906, 2016.

[13] Bannari, A. *et al.* "Sentinel-MSI VNIR and SWIR Bands Sensitivity Analysis for Soil Salinity Discrimination in an Arid Landscape". *Remote Sensing*, 10(6), 855; 2018.

[14] El-Battay, A. *et al.* "Comparative Study among Different Semi-Empirical Models for Soil Salinity Prediction in an Arid Environment Using OLI". *Adv. in Remote Sens.,* 6, 23-39, 2017.

[15] Al-Sarawi, M. *et al.* "Geomorphologic Controls on Surface Deposits of Kuwait as Depicted in Satellite Images". Kuwait *J. of Sci. Eng.* 33 (2), 123-154, 2006.

[16] Al-Sarawi, M. "Surface Geomorphology of Kuwait". *Geo. Journal,* 35(4), 493-503, 1995.

[17] Al-Sarawi, M. "Introduction of Geomorphologic Provinces in Kuwait's Desert Using Multi-Source and Multi-Data Satellite Data". Proc. of the Eleventh Thematic Conference and workshops on Applied Geological Remote Sensing, 27-29 February, Las Vegas, Nevada, pp. 536-545, 1996.

[18] Milton, D. "Geology of the Arabian Peninsula, Kuwait, Geological Survey Professional Paper". Washington: United State Government Printing Office, 1967.

[19] Omar, S. and Shahid, S. "Reconnaissance Soil Survey for the State of Kuwait". In S. Shahid, F. Taha, and M. Abdelfattah, Developments in Soil Classification, Land Use Planning and Policy Implications: Innovative Thinking of Soil Inventory for Land Use Planning and Management of Land Resources (pp. 85-107). Springer Science + Business Media Dordrecht, 2013.

[20] USDA. "Soil Taxonomy: A basic System of Soil Classification for making and Interpreting Soil Surveys". USA: United States Department of Agriculture, 1999.

[21] USDA-NRCS "Soil Survey Laboratory Methods Manual". Soil Survey Investigations Report, No.42 Version 4, 2004.

[22] Pahlevan, N. *et al.* "On-Orbit Radiometric Characterization of OLI (Landsat-8) for Applications in Aquatic Remote Sensing". *R. S. of Envi., 154,* 272-284, 2014.

[23] Bannari, A. *et al.* "Nécessité de l'étalonnage radiométrique et standardisation des données de télédétection". *Canadian J. of Remote Sensing*, 25 (1), 45-59, 1999.

[24] Teillet, P. *et al.* "Sensitivity of Surface Reflectance Retrieval to Uncertainties in Aerosol Optical Properties". *Applied Optics,* 33 (18), 3933-3944, 1994.

[25] Teillet, P. and Santer, R. "Terrain Elevation and Sensor Altitude Dependence in a Semi-Analytical Atmospheric Code". *Canadian J. of Remote Sensing,* 17 (1), 36-44, 1991.

[26] PCI-Geomatica *"Using PCI Software".* Richmond Hill, Ontario, Canada, 540 pages, 2017.

[27] Wu, W. *et al.* "Soil Salinity Mapping by Multiscale Remote Sensing in Mesopotamia, Iraq". *IEEE J. of Sel. Topics in Applied E.O. and R.S.*, 7(11), 4442-4452, 2014.

[28] Fernandez-Buces, N. *et al.* "Mapping Soil Salinity Using a Combined Spectral Response Index for Bare Soil and Vegetation: A Case Study in the Former Lake Texcoco, Mexico". *Journal of Arid Environments,* 65(4), 644-667, 2006.

[29] El-Harti, A. *et al.* "Spatiotemporal Monitoring of Soil Salinization in Irrigated Tadla Plain (Morocco) Using Satellite Spectral Indices". *Int. J. of Applied Earth Observation and Geoinformation,* 50, 64-73, 2016.

[30] Asfaw, E. *et al.* "Soil Salinity Modeling and Mapping Using Remote Sensing and GIS: The Case of Wonji Sugar Cane Irrigation Farms, Ethiopia". *Journal of the Saudi Society of Agricultural Sciences,* 1-9, 2016.

[31] Bannari, A. *et al.* "Salt-Affected Soil Mapping in an Arid Environment using Semi-Empirical Model and Landsat-OLI Data". *Advances in Remote Sensing,* 6, 260-291, 2017.

[32] Willmott, C.J. "Some comments on the evaluation of model performance". *Bulletin American Meteorological Society, 63 (11),* 1309-1313, 1982.

[33] Bannari, A. *et al.* " Effets de la couleur et de la brillance du sol sur les indices de végétation". *Int. J. of R. Sensing, 17(10),* 1885-1906, 1996.